Analysis Of The Microgrid's Frequency Resilience Using A Lightweight Selfish Sheep Optimisation Algorithm

Anjiang Liu*, Youzhuo Zheng, Di Weng, Hengrong Zhang, and Xinhao Li

Electric Power Research Institute, Guizhou Power Grid Co., Ltd, Guiyang, 550002, China

**Corresponding author. E-mail: leeli@hust.edu.cn*

Received: Mar. 19, 2026; Accepted: Apr. 23, 2026

The lightweighting problem in microgrid (MG) simulation models is first officially described in this paper as an optimisation assignment with the goal of minimising the disturbances to the microgrid frequency robustness. This paper formally presents the lightweighting problem in microgrid (MG) simulations as an optimization task aimed at minimizing frequency disturbances. We propose a Selfish Herd Optimization (SHO)-based technique and its FA-SHO enhancement, using group and predator parameters to model prey–predator interactions. The algorithms optimize gain values and controllers to improve system robustness. Experimental results show that FA-SHO outperforms SHO, with faster convergence, lower error metrics, and better frequency response, while the SMC ensures strong dynamic stability and resilience.

Keywords: microgrid, lightweight algorithm, selfish flock optimization, voltage stability control, SHO algorithm, FA-SHO algorithm

http://dx.doi.org/10.6180/jase.202611_34.029

1. Introduction

Microgrids are flexible solutions for integrating renewable energy, using local resources like solar, wind, storage, and conventional generators to improve energy management, load control, and reliability [1]. High renewable penetration introduces load variability and uncertainty, affecting stability [2], and challenges remain in voltage stability, control optimization, and system integration [3]. Key considerations include operation in virtual, islanded, and grid-connected modes, incorporating market and wind forecasts, handling three-phase imbalances, and managing parameter, topological, and frequent load or generation changes. Control strategies include centralized, master-slave, and sag control, each with trade-offs in communication needs and stability [4, 5]. The Selfish Flock Optimization (SFO) technique offers fast convergence, global optimality, and robust disturbance handling, enabling lightweight modelling and efficient simulation [6]. This paper analyses load impacts and proposes an SFO-based control method to enhance voltage stability, power quality, and robustness at lower cost.

2. Microgrid simulation models' lightweighting for selfish flock optimisation

2.1. Lightweighting issues

The microgrid simulation model lightweighting problem, also known as the mathematical model employing intelligent optimisation, is first officially presented in this section [7, 8]. Here, lightweighting is defined as a computational model reduction approach that reduces simulation complexity while preserving essential dynamics and frequency response accuracy. It can be summed up as follows: as the optimisation goal, i.e., the least amount of points and surfaces produced by the microgrid simulation:

$$\min\left(W=\sum_{i=1}^{n} f_w\left(x_i\right)\sigma_i^0\right),$$
$$x=\left(x_1,x_2,\cdots,x_n\right)\ \text{s.t.}\ \begin{cases}\sigma_{ij}\leqslant f_\sigma\left(x_i\right)\sigma_i^0\\ \lambda_{ij}\left(f_w\left(x_i\right),f_w\left(x_j\right)\right)\leqslant\lambda_i\\ 0\leqslant x_j\leqslant x_i\leqslant 1\\ j=1,2,\cdots,l\quad i=1,2,\cdots,n\end{cases} \tag{1}$$

N is the total number of faces, σ_{ij} the number of points in face i of the $\mathrm{j^{th}}$ 3D mesh, λ_{ij} the texture density constraint, ${\sigma_{\mathrm{i}}}^0$ and λ_{i} the constraint eigenvalues, and fw (x_j) constructs face i using point x,i. Global constraints can be adjusted to speed optimization convergence, while local point-face and texture constraints define the overall constraints as follows:

$$\sum_{i=1}^{n}\left(x_i^{(k)}\right)^{\beta} e_{ij}^{(k)}/x_i^{\beta}\leqslant\bar{e}_j(j=1,2,\cdots,l) \tag{2}$$

where $e_{ij}^{(k)}$ is the topological variable obtained after the constraint on the number of points on the ith face in the jth 3D mesh and the kth iteration, which can be handled according to the redundancy of the various 3D networks, and also according to the required strain energy [9, 10]. In the lightweight MG formulation, the decision variables physically correspond to the retained equivalent states, interconnection nodes, and subsystem coupling links representing DG units, renewable sources, storage branches, and controllable loads.

2.2. An explanation of a simple technique

The Selfish Flock Optimisation (SFO) method, proposed by Fausto in 2017, is a metaheuristic inspired by Hamilton's Selfish Flock Theory [11, 12]. It models prey-predator interactions with two groups-hunted and hunting-using evolutionary operators in the solution space to mimic behavior and find optimal solutions [13].

(1) Initialize population individuals

In the SFO method, the population S, consists of N individuals, each representing positions in the solution space. Each individual is defined as $S_i=\left(s_{i,1},s_{i,1},\ldots,s_{i,n}\right)$, where n is the problem size. For simulations, the population size is set to 100 with a maximum of 100 iterations. Constraints are handled by initializing individuals within predefined upper and lower bounds. The following is the initialization formula for the entire population group:

$$s_{i,j}=x_j^{\text{low}}+\operatorname{rand}(0,1)\cdot\left(x_j^{\text{high}}-x_j^{\text{low}}\right) \tag{3}$$

where the solution space's top and lower boundaries are indicated, respectively, by x_j^{low} and x_j^{high}. The random function $S=(H\cup P)$ produces results whose range lies inside the interval [0, 1].

In the Selfish Herd Optimisation (SHO) algorithm, the population S is divided into prey (H) and predators (P), with PS $=$ H$\cup$P. Typically, more prey exists than predators; in SHO, 70%-90% of individuals are prey (N_h) and the rest are predators (N_p). Nh and Np are determined using the following formula [14].

$$N_h=floor(N\cdot\operatorname{rand}(0.7,0.9)) \tag{4}$$

$$N_p=N-N_h \tag{5}$$

where rand () is a random number with values ranging from 0.7 to 0.9 and floor (•) is a function that converts real numbers into integers [15].

(2) Allocation of survival value

The capacity of an individual to either successfully kill prey in an attack or to survive an attack is represented by the survival value SV_{s_i} that is assigned to each individual (s_i) of the total population (S) in SHO [16, 17]. The following is the definition of the survival value mathematical formula:

$$SV_{s_i}=\frac{f\left(s_i\right)-f_{\text{worst}}}{f_{\text{best}}-f_{\text{worst}}} \tag{6}$$

where f_{best} and f_{worst} denote the objective function's best and worst values, respectively, and f($\cdot$) stands for the objective function. Seventy to ninety percent of the prey had survival values evaluated; the prey leader had the greatest value, while the easiest-to-catch prey had the lowest.

3. Control of voltage stabilisation in microgrid systems

This work designs SHO and FA-SHO based controllers to improve robustness and dynamic performance. The ITAE objective function minimizes error for faster settling and reduced oscillations [18]. Stability is ensured using a state-space method with coupled Riccati equations solved in MATLAB. ITAE provides better performance balance compared to IAE, ISE, and ITSE. The following illustrates how the gain/scaling factor's boundary values constrain the optimisation problem:

$$J_{0\_\text{ITAE}}=\begin{cases}\int_0^T t\left[\left|\Delta f_1\right|\right]dt\\ \int_0^T t\left[\left|\Delta f_1\right|+\left|\Delta f_2\right|+\left|\Delta p_{\text{tie}}\right|\right]dt\end{cases} \tag{7}$$

$$(kps_{\min^m},kin_{\min^m},kdf_{\min^m})<(kpr,kin,kdf)<(kpr_{\max^m},kn_{\max^m},kdf_{\max^m})\,(\gamma_{\min^m},\zeta_{\min^m})<(\gamma,\zeta)<(\gamma_{\max^m},\zeta_{\max^m})$$

and

$$\left(\alpha_{gn\ min^m}, \phi_{m\,\min^m}, k_{slmc}min^m\right) < \left(\alpha_{gn}, \phi_m, k_{slmc}\right)$$
$$< \left(\alpha_{gn\,\max^m}, \phi_{m\,\max^m}, k_{slmc\,\max^m}\right)$$

are the respective boundary values for the SMC scaling factor, FO value, and classical controller gain. Here, max and min, m denote the upper and lower bounds. For the classical controller, gains range from 0.001 to 50, while for the SMC controller, they vary from -5 to 150. The SMC sliding surface is designed using voltage error and its derivative to ensure fast convergence and robust performance. Mathematically, the sliding surface is defined as

$$s(t) = \alpha e(t) + \dot{e}(t) \tag{8}$$

where $e(t)$ is the voltage error and α is a positive design constant. The reaching condition is governed by the Lyapunov stability criterion $s(t) < 0$, ensuring finite-time convergence to the sliding surface. The microgrid control architecture consists of three layers: system, centralized, and local control, working together for energy optimization and maintaining voltage and frequency stability.

(1) It uses a combination of load models-constant current (I), constant power (P), and constant impedance (Z)-to accurately represent real microgrid load behavior. The comparative results confirmed consistent voltage-dependent active and reactive power behaviour, demonstrating that the proposed formulation accurately preserves the practical response characteristics of composite microgrid loads. Furthermore, the static load model needs to fulfil

$$P = P_0\left[a_p\left(U/U_0\right)^2 + b_p\left(U/U_0\right) + c_p\right] \tag{9}$$

$$Q = Q_0\left[a_q\left(U/U_0\right)^2 + b_q\left(U/U_0\right) + c_q\right] \tag{10}$$

$$a_p + b_p + c_p = 1 \tag{11}$$

$$a_q + b_q + c_q = 1 \tag{12}$$

Where: U and U_0 are, respectively ctual and reference voltage, while P and Q, and P_0, Q_0 denote load power at respective voltages. The ZIP model combines constant power, current, and impedance components with coefficients reflecting practical load behavior. Reactive power shares are defined by coefficients a_q, b_q, c_q induction motor dynamics are modeled using a third-order equation, assuming load varies with the square of speed. The mathematical model for it is:

$$\left\{\begin{array}{rl} \frac{dE'_d}{dt} &= -\frac{1}{T'}\left[E'_d + \left(X - X'\right)I_q\right] - (\omega - 1)E'_q \\ \frac{dE'_q}{dt} &= -\frac{1}{T'}\left[E'_q + \left(X - X'\right)I_d\right] - (\omega - 1)E'_d \\ \frac{d\omega}{dt} &= -\frac{1}{2H}\left[\left(A\omega^2 + B\omega + C\right)T_0 - \left(E'_d I_d + E'_q I_q\right)\right] \end{array}\right. \tag{13}$$

$$\left\{\begin{array}{l} I_d = \frac{1}{R_S^2 + X'^2}\left[R_S\left(U_d - E'_d\right) + X'\left(U_q - E'_q\right)\right] \\ I_q = \frac{1}{R_S^2 + X^{22}}\left[R_s\left(U_q - E'_q\right) - X'\left(U_d - E'_d\right)\right] \end{array}\right. \tag{14}$$

$$\begin{aligned} T' &= \left(X_r + X_m\right)/R_r \\ X &= X_s + X_m \\ X' &= X_s + X_m X_r/\left(X_m + X_r\right) \\ A &+ B + C = 1 \end{aligned} \tag{15}$$

The T_0 and q-axis components of the stator current of the induction motor are shown by the numbers I_d and I_q, the symbols $E'_d, E'_q; X'$ is the transient reactance of the induction motor, and T′ is the transient potential decay time constant.

(2) Develop the diesel generator's mathematical model for the AC brushless excitation system:

$$\begin{aligned} \dot{E} &= AE + B_1 I + B_2 u \\ y &= \mathrm{CE} \end{aligned} \tag{16}$$

$$E = \begin{bmatrix} E_{fd} \\ E'_q \\ E''_q \\ E''_d \end{bmatrix}, \quad A = \begin{bmatrix} -\frac{1}{T_l} & 0 & 0 & 0 \\ \frac{1}{T_{d0}} & -\frac{1}{T_{d0}} & 0 & 0 \\ \frac{c}{T_{d0}} & \frac{1}{T''_{d0}} - \frac{c}{T_{d0}} & -\frac{1}{T''_{d0}} & 0 \\ 0 & 0 & 0 & -\frac{1}{T''_{q0}} \end{bmatrix} \tag{17}$$

where E'_q is the transient electromotive force; E''_q and E''_d are the sub-transient electromotive force's straight-axis (d-axis) and transverse-axis (q-axis), respectively; and E_{fd} is the electromotive force in relation to the voltage of the generator's excitation coil $\left(U_f\right)$.

(3) Using the load model as disturbance and the diesel generator excitation system as the plant, the closed-loop control maintains microgrid voltage stability. The robust controller is designed via the "2-Riccati equation" method, with evaluation signals $z_1 - z_3$ weighted by $W_1 - W_3$ to enforce performance, limit uncertainty, and constrain controller signals. The hybrid sensitivity framework incorporates these weightings as follows:

$$\begin{bmatrix} W_1 e \\ W_2 u \\ W_3 y \\ e \end{bmatrix} = \begin{bmatrix} W_1 & -W_1 G \\ 0 & W_2 \\ 0 & W_3 G \\ I & -G \end{bmatrix}\begin{bmatrix} r \\ u \end{bmatrix} = P_0\begin{bmatrix} r \\ u \end{bmatrix} \tag{18}$$

where G represents the diesel generator AC brushless excitation system, and P_0 is the synchronous generator model. The reference and control inputs are defined accordingly. The closed-loop system satisfies $\|P\| < 1$, for robust stability, where $P = \begin{bmatrix} W_1 S \\ W_2 R \\ W_3 T \end{bmatrix}$ where $W_1 S$ denotes a performance restriction on the closed-loop control system's complementary sensitivity function is represented by T, and $W_1 S$ highlights the need for the closed-loop control system to have strong stability, which satisfies $||W_3 S|| < 1$. The robust controller for voltage stabilisation is K.

4. result

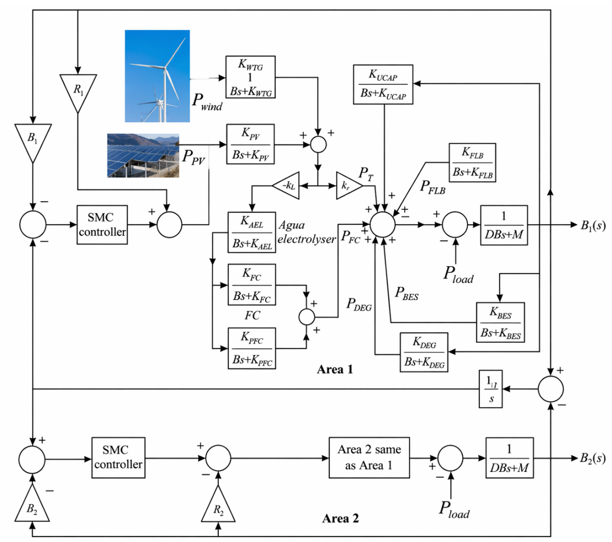

Fig. 1. MG model for analysis of frequency stability.

The MG model (Fig. 1) was simulated in MATLAB/Simulink R2016a, integrating diesel generator, PV, wind, FC-AEL, controllable load, and energy storage via a common AC bus. Using a 0.01 s fixed-step solver for 120 s, simulations captured fast transients, renewable intermittency, and step-load disturbances. Stochastic models and benchmark functions evaluated FA-SHO's performance advantage over SHO across different controller settings in Fig. 2.

4.1. Using benchmarking functions, examine how the suggested FA-SHO method performs in comparison to the SHO algorithm

FA-SHO and SHO were tested on 10 benchmark functions (30 runs, 100 population, 100 iterations). FA-SHO converges faster with better statistical results (mean, best, worst, and SD at 95% confidence). Mamdani fuzzy logic

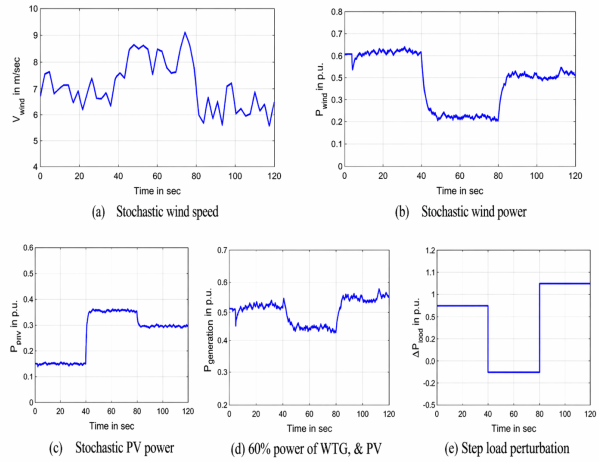

Fig. 2. Step/random curves for loads, WG/PV power, and wind speed.

helps FA-SHO balance exploration and exploitation, while SHO provides stronger global search [19].

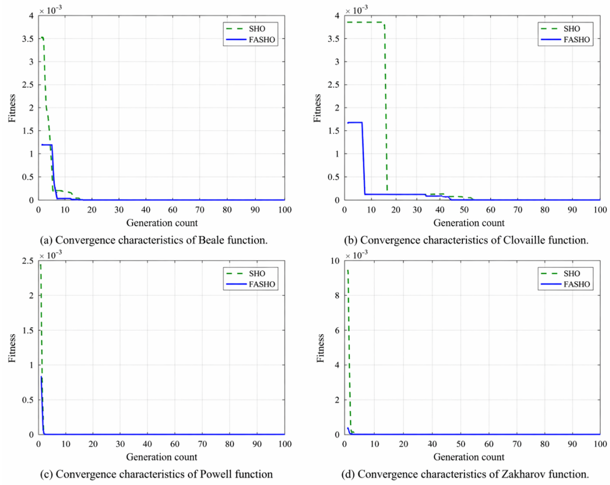

Fig. 3. Convergence properties.

4.2. Performance in Regional MG

The frequency response of microgrids was evaluated using GOA- and SHO-based PID, FOPID, and FOPID-(1+PI) controllers under identical conditions, ensuring differences arise solely from the optimization algorithm [20]. Table 3 lists the gain parameters, and Fig. 4 shows that SHO-based controllers outperform GOA-based ones.

Leveraging SHO's superiority over GOA, this work enhances robustness against renewable energy uncertainties. Stochastic wind and solar models supply 60% to the MG and 40% to FC-AEL hydrogen storage. Under three 40 s disturbances, SHO-SMC achieves lower frequency devia-

Table 1. An explanation of the study's benchmarking function.

Name of the function	Functions expression	Dimension	Search space
Bohachevsky 1	$F_1 = x_1^2 + 2x_2^2 - 0.3\cos(2\pi x_1) - 0.4\cos(4\pi x_2) + 0.7$	2	[100,100]
Beale	$F_2 = (1.5 - x_1 + x_1 x_2)^2 + \left(2.25 - x_1 + x_1 x_2^2\right)^2$	2	[-4.5,4.5]
Branin	$F_3 = \left(x_2 - \frac{5.1}{4\pi} x_1^2 + \frac{5}{4\pi} x_1 - 6\right)^2 + 10\left(1 - \frac{1}{8\pi}\right)\cos x_1 + 10$	2	[-5,10]
Clovaille	$F_4 = 100\left(x_1^2 - x_2\right)^2 + (x_1 - 1)^2 + (x_3 - 1)^2 + 90\left(x_3^2 - x_4\right)^2 + 10.1\left((x_2 - 1)^2 + (x_4 - 1)^2\right) + 19.8\,(x_2 - 1)\,(x_4 - 1)$	4	[-10,10]
Dixon-price	$F_5 = (x_i - 1)^2 + \sum_{i=2}^{n} i\left(2x_i^2 - x_{i-1}\right)^2$	30	[-10,10]
Rastigin	$F_9 = \sum_{i=1}^{n}\left[x_i^2 - 10\cos(2\pi x_i)\right] + 10$	30	[5.12,5.12]
Zakhrow	$F_{10} = \sum_{i=1}^{n} x_i^2 + \left(\sum_{i=1}^{n} 0.5 i x_i\right)^2 + \left(\sum_{i=1}^{n} 0.5 i x_i\right)^4$	30	[-30,30]

Table 2. Performance Evaluation of the SHO and FASHO Algorithms.

Algorithm	Function	Optimum value	Minimum	Maximum	Mean	Standard deviation	Computational time (s)
SHO	F_1	0	0	0	0	0	0.033
FA-SHO			0	0	0	0	0.028
SHO	F_2	0	0	0	0	0	0.029
FA-SHO			0	0	0	0	0.068
SHO	F_3	0.395	0.398	0.398	0.399	0	0.064
FA-SHO							
SHO	F_4	0	2.456	4.266	1.145	1.256	0.026
FA-SHO			1.565	4.562	0.398	0	0.035
SHO	F_5	0	0.667	0.666	0.667	0	1.732
FA-SHO			0.668	0.667	0.667	0	1.732

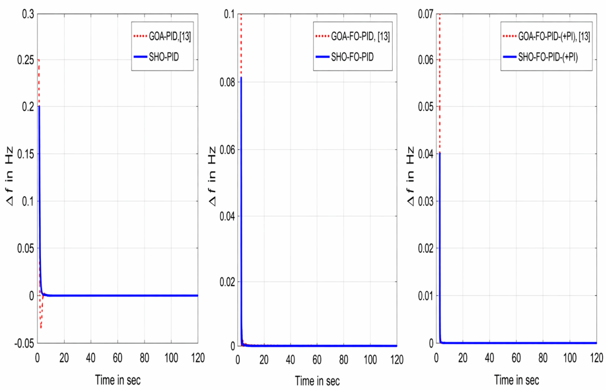

Fig. 4. Comparison of the GOA-FOPID and SHO-FOPID frequency responses.

tion (0.0153 Hz) with better settling time, overshoot, and sag compared to other methods, highlighting its superior dynamic performance (Table 4 and Fig. 5) [21].

The SHO-SMC outperforms SHO, and FA-SHO further enhances performance. FA-SHO-SMC shows lower frequency deviations and faster response under uncertainties, proving its superiority (Tables 4 and 5, Fig. 5(b)).

4.3. Bi-Regional MG Medium Performance

A two-zone microgrid was simulated in MATLAB to assess controller stability and the FA-SHO algorithm. The FA-SHO-SMC controller outperformed others, showing faster response, lower overshoot (2.1198 mHz in region 1). Rapid stabilization of frequency and tieline power (Δf_2, ΔP_{tie}), confirming its superior performance and adaptability (Fig. 6 and Table 6).

Table 3. Otimal controller gain parameters.

Controller/algorithm		kpr	kin	kdf	γ	k_{simc}
SHO	PID	13.264	4.214	12.958	-	-
	FOPID	36.254	39.585	11.265	-	-
	SMC	-	-	-	50.212	47.034
FASHO	PID	18.501	5.945	19.587	-	-
	FOPID	39.564	45.000	20.145	-	-
	SMC	-	-	-	-	125.58

Table 4. Frequency deviation transient parameters (downshoot, overshoot, and stabilisation time).

Controller	FASHO				SHO			
	U_s(Hz)	O_s(Hz)	ts(s)	ITAE	U_s(Hz)	O_s(Hz)	ts(s)	ITAE
PID	-0.158	0.143	1.93	0.065	-0.021	0.1885	2.29	0.1015
FOPID	0	0.367	1.54	0. 035	-0.002	0.0867	1.94	0.0354
SMC	0	0.025	0.41	0.005	0	0.0214	0.23	-

Table 5. Optimal gain parameters for the controller.

Controller/algorithm			kpr	kin	kdf	γ	k_{simc}
SHO	FOPID(1+P)	Cont 1	2.945	2.524	1.024	0.135	-
	SMC	Cont 2	2.358	1.032	2.036	0.464	-
FASHO	FOPID(1+P)	Cont 1	2.501	1.036	2.564	0.451	-
	SMC	Cont 2	2.267	2.254	1.947	1.908	-

Table 6. Optimal gain parameters for the controller.

Indices	SHO-FOPID-(1+P)			FA+SHO-FOPID-(1+P)			SHO-SMC			FA-SHO-SMC		
	Δf_1	Δf_2	Δf_{pie}	Δf_1	Δf_2	Δf_{pie}	Δf_1	Δf_2	Δf_{pie}	Δf_1	Δf_2	Δf_{pie}
U_s	36.3 3	183.5	-32.34	27.45	126.71	-54.068	-18.89	-13.73	-13.45	-10.35	-12.03	-0.487
O_s	15.5 2	85.69	265.31	15.26	59.64	130.54	1.825	2.456	0.178	1.1998	0.802	0.335
t_s	6.24 1	3.525	2.865	6.421	2.125	3.824	0.265	0.214	0.188	0.013	0.036	0.017

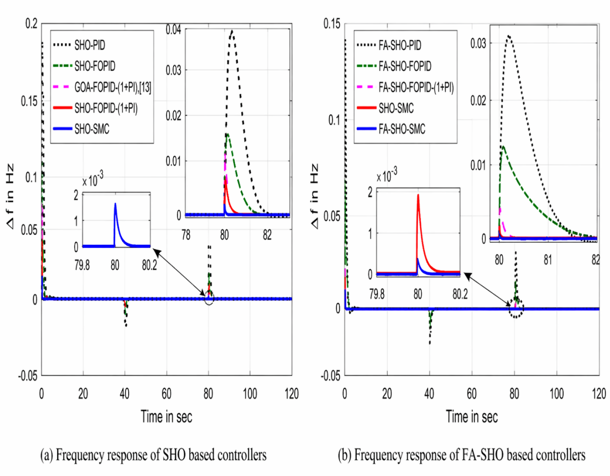

Fig. 5. Different controllers' frequency responses created using SHO and FA-SHO algorithms.

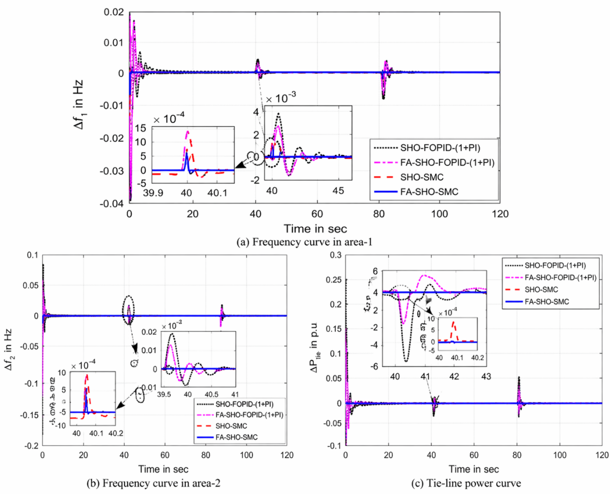

Fig. 6. Expert panel's dynamic response in a two-region polygon.

4.4. Sturdiness of the FA-SHO-SMC controller suggestion: feasibility

To verify robustness, additional uncertainties such as communication delays, random loads, and parameter variations are considered along with RES uncertainties, and their impacts are analysed [22].

4.4.1. Communications delay

Communication delays (2 ms) were modeled and compensated, with the FA-SHO-SMC controller rapidly stabilizing frequency and tie-line power while slightly outperforming SHO. Higher switching gains improve disturbance rejection but may increase oscillations, showing a trade-off between performance and smoothness in Fig. 7.

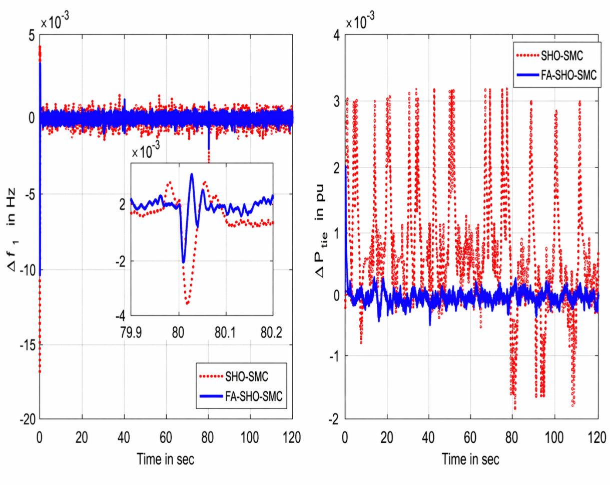

Fig. 7. Dynamic response with delay.

4.4.2. When the load changes suddenly

In Fig. 8(c), the stochastic renewable energy model and step-load perturbations are applied in region 1. Fig. 8(a) and (b) show that FA-SHO-SMC significantly reduces Δf_1 and Δf_{pie} peaks compared to SHO-SMC, maintaining stable performance even under sharp load changes.

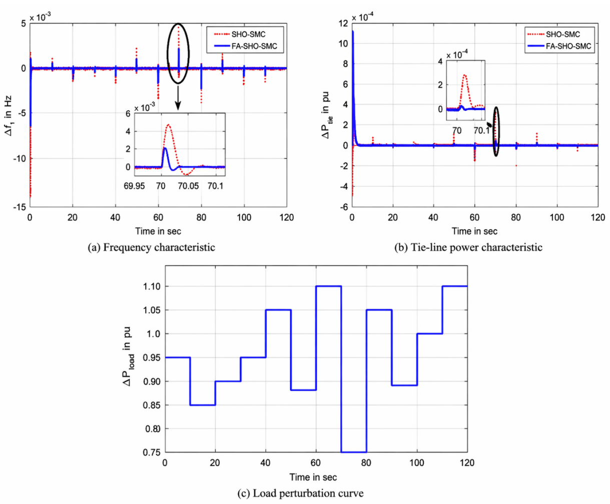

Fig. 8. Dynamic reaction to sudden changes in load.

4.4.3. Communication delays and load surges

The SMC controller remained robust under rapid load changes and communication delays, with Δf_1 and Δf_{pie} showing minimal variation. Load fluctuations had less impact than delays, confirming stable system performance in Fig. 9.

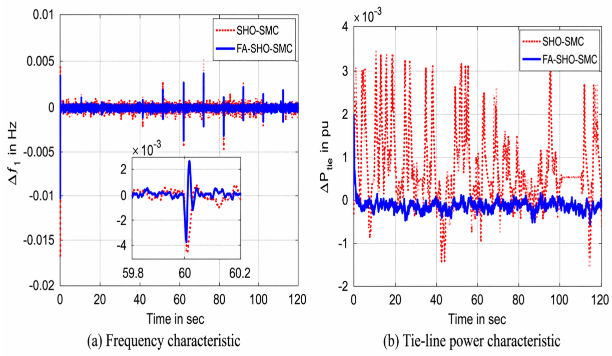

Fig. 9. Dynamic reaction to sudden changes in load and time delays.

4.5. As the various compositional factors in MG vary

The microgrid remained stable under 50% parameter variations and time delays, with FA-SHO-SMC showing minor chattering for faster stabilization. Without delays or variations, the system exhibited smooth and robust performance (Fig. 10(a)-(j)).

5. Conclusion

This work proposes a lightweight SHO-based method with a robust controller for microgrid voltage stability. Simulation and statistical results (t-test, ANOVA) show improved stability and performance compared to existing methods. The approach can be extended to larger systems, with future work focusing on computational efficiency.

Declarations

Conflicts of Interest

The authors declare that they have no conflict of interest.

Ethical Approval

This article does not contain any studies with human participants or animals performed by any of the authors.

Consent to Participate

Not applicable.

Consent for Publication

Not applicable.

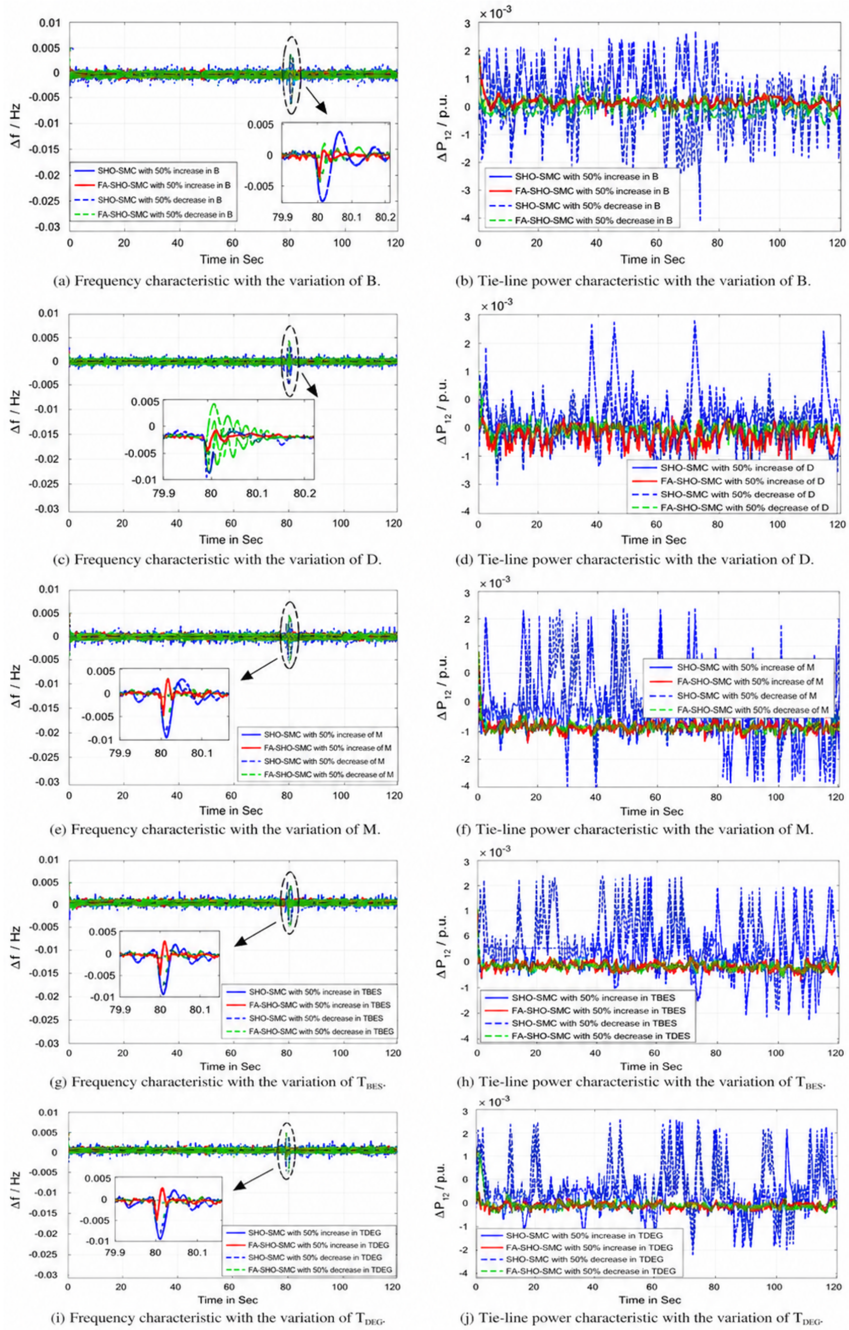

Fig. 10. Dynamic reaction with time lag and parameter modification.

Availability of Data and Materials

The data supporting the findings of this study are available from the corresponding author upon reasonable request.

Author Contributions

Anjiang Liu conceived and supervised the study. Youzhuo Zheng collected data, Di Weng handled software and analysis, Hengrong Zhang supported methodology and validation, and Xinhao Li drafted the manuscript. All authors approved the final version.

References

[1] K. Han, K. Yang, and L. Yin, (2022) *"Lightweight Actor-Critic Generative Adversarial Networks for Real-Time Smart Generation Control of Microgrids"* **Applied Energy *317***: 119163. DOI: 10.1016/j.apenergy.2022.119163.

[2] S. Lu and X. Li, (2021) *"Quantum-Resistant Lightweight Authentication and Key Agreement Protocol for Fog-Based Microgrids"* **IEEE Access** ***9***: 27588–27600. DOI: 10.1109/ACCESS.2021.3058180.

[3] S. Leonori, A. Martino, F. M. F. Mascioli, and A. Rizzi, (2020) *"Microgrid Energy Management Systems Design by Computational Intelligence Techniques"* **Applied Energy** ***277***: 115524. DOI: 10.1016/j.apenergy.2020.115524.

[4] C. Xia, W. Li, X. Chang, T. Yang, and A. Y. Zomaya, (2023) *"A Rank-Based Multiple-Choice Secretary Algorithm for Minimising Microgrid Operating Cost under Uncertainties"* **Frontiers in Energy** ***17***(2): 198–210. DOI: 10.1007/s11708-023-0874-8.

[5] R. Kumar and N. Sinha, (2021) *"Voltage Stability of Solar Dish-Stirling Based Autonomous DC Microgrid Using Grey Wolf Optimised FOPID-Controller"* **International Journal of Sustainable Energy** ***40***(5): 412–429. DOI: 10.1080/14786451.2020.1806843.

[6] M. Bhuyan, A. K. Barik, and D. C. Das, (2020) *"GOA Optimised Frequency Control of Solar-Thermal/Sea-Wave/Biodiesel Generator Based Interconnected Hybrid Microgrids with DC Link"* **International Journal of Sustainable Energy** ***39***(7): 615–633. DOI: 10.1080/14786451.2020.1741589.

[7] M. Shehab, L. Abualigah, H. Al Hamad, H. Alabool, M. Alshinwan, and A. M. Khasawneh, (2020) *"Moth–Flame Optimization Algorithm: Variants and Applications"* **Neural Computing and Applications** ***32***(14): 9859–9884. DOI: 10.1007/s00521-019-04570-6.

[8] N. V. Rajeesh Kumar, N. Jaya Lakshmi, B. Mallala, and V. Jadhav, (2023) *"Secure Trust Aware Multi-Objective Routing Protocol Based on Battle Competitive Swarm Optimization in IoT"* **Artificial Intelligence Review** ***56***(Suppl 2): 1685–1709. DOI: 10.1007/s10462-023-10560-x.

[9] J. Heidary, M. Gheisarnejad, H. Rastegar, and M. H. Khooban, (2022) *"Survey on Microgrids Frequency Regulation: Modeling and Control Systems"* **Electric Power Systems Research** ***213***: 108719. DOI: 10.1016/j.epsr.2022.108719.

[10] C. Zhang, G. Shan, B. H. Roh, F. Zhu, and J. Jiang, (2026) *"FEI-Hi: Federated Edge Intelligence for Healthcare Informatics"* **IEEE Journal of Biomedical and Health Informatics** ***30***(3): 1853–1866. DOI: 10.1109/JBHI.2025.3588551.

[11] C. Zhang, B. H. Roh, and G. Shan, (2024) *"Federated Anomaly Detection"* **Proceedings of the 54th Annual IEEE/IFIP International Conference on Dependable Systems and Networks – Supplemental Volume (DSN-S)**: 148–149.

[12] N. K. Jena, S. Sahoo, B. K. Sahu, and K. B. Mohanty, (2021) *"Frequency Stability Analysis with Fuzzy Adaptive Selfish Herd Optimization Based Optimal Sliding Mode Controller for Microgrids"* **International Journal of Emerging Electric Power Systems** ***22***(5): 547–568. DOI: 10.1515/ijeeps-2021-0105.

[13] A. Saha, P. Dash, N. R. Babu, T. Chiranjeevi, M. Dhananjaya, and Ł. Knypiński, (2022) *"Dynamic Stability Evaluation of an Integrated Biodiesel-Geothermal Power Plant-Based Power System with Spotted Hyena Optimized Cascade Controller"* **Sustainability** ***14***(22): 14842. DOI: 10.3390/su142214842.

[14] A. Yimit, K. Iigura, and Y. Hagihara, (2020) *"Refined Selfish Herd Optimizer for Global Optimization Problems"* **Expert Systems with Applications** ***139***: 112838. DOI: 10.1016/j.eswa.2019.112838.

[15] D. W. Sankey, R. F. Storms, R. J. Musters, T. W. Russell, C. K. Hemelrijk, and S. J. Portugal, (2021) *"Absence of 'Selfish Herd' Dynamics in Bird Flocks under Threat"* **Current Biology** ***31***(14): 3192–3198. DOI: 10.1016/j.cub.2021.05.009.

[16] R. Zhao, Y. Wang, G. Xiao, C. Liu, P. Hu, and H. Li, (2022) *"A Method of Path Planning for Unmanned Aerial Vehicle Based on the Hybrid of Selfish Herd Optimizer and Particle Swarm Optimizer"* **Applied Intelligence** ***52***(14): 16775–16798. DOI: 10.1007/s10489-021-02353-y.

[17] G. G. Wang, C. L. Wei, Y. Wang, and W. Pedrycz, (2021) *"Improving Distributed Anti-Flocking Algorithm for Dynamic Coverage of Mobile Wireless Networks with Obstacle Avoidance"* **Knowledge-Based Systems** ***225***: 107133. DOI: 10.1016/j.knosys.2021.107133.

[18] A. Villalón, M. Rivera, Y. Salgueiro, J. Muñoz, T. Dragičević, and F. Blaabjerg, (2020) *"Predictive Control for Microgrid Applications: A Review Study"* **Energies** ***13***(10): 2454. DOI: 10.3390/en13102454.

[19] R. Trivedi and S. Khadem, (2022) *"Implementation of Artificial Intelligence Techniques in Microgrid Control Environment: Current Progress and Future Scopes"* **Energy and AI** ***8***: 100147. DOI: 10.1016/j.egyai.2022.100147.

[20] S. P. Bihari, P. K. Sadhu, K. Sarita, B. Khan, L. D. Arya, R. K. Saket, and D. P. Kothari, (2021) *"A Comprehensive Review of Microgrid Control Mechanism and Impact Assessment for Hybrid Renewable Energy Integration"* **IEEE Access** ***9***: 88942–88958. DOI: 10.1109/ACCESS.2021.3090266.

[21] J. Ali, R. H. Jhaveri, M. Alswailim, and B. H. Roh, (2023) *"ESCALB: An Effective Slave Controller Allocation-Based Load Balancing Scheme for Multi-Domain SDN-Enabled IoT Networks"* **Journal of King Saud University–Computer and Information Sciences** ***35***(6): 101566. DOI: 10.1016/j.jksuci.2023.101566.

[22] A. Dinesh and J. Rangaraj, (2025) *"An Energy-Efficient Routing Protocol for Wireless Body Area Networks Using Hybrid Artificial Bee Colony Optimization and Chicken Swarm Optimization Algorithm"* **Journal of Engineering and Applied Science** ***72***(1): 45. DOI: 10.1186/s44147-024-00533-4.